Astron. Astrophys. 360, 707–714 (2000)

ASTRONOMY AND ASTROPHYSICS

Turbulent *f*-mode in a stratified solar atmosphere

K. Murawski

Technical University of Lublin, Department of Environmental Physics, ul. Nadbystrzycka 40, 20-618 Lublin, Poland

Received 20 September 1999 / Accepted 28 January 2000

Abstract. The solar *f*-mode is a surface gravity wave which high horizontal wavenumber k and the frequency ω satisfy the dispersion relation $\omega^2 = gk$, where g is the surface gravity of the Sun. However, the observations of this mode revealed deviations from this simple dispersion relation. According to these observations for high values of k the *f*-mode frequency is significantly lower than the frequency given by the simple dispersion relation and the line-width grows with k.

We derive a general dispersion equation which is valid for arbitrary vertical profiles of the stratified solar atmosphere. As an illustrative example the case of isothermal atmosphere is considered. Solving this equation numerically for various parameters of the equilibrium and the turbulent flow we find that the frequencies and line-widths of the turbulent *f*-mode are close to those observed recently by the SOHO/MDI.

Key words: convection – Sun: atmosphere – Sun: granulation – Sun: oscillations – turbulence

1. Introduction

The classical *f*-mode (*f* stands for fundamental) is recognized as a compressionless wave that propagates in an inviscid atmosphere that is permeated by constant gravity field (e.g., Campbell & Roberts 1989). Its frequency ω_0 is given by the following dispersion relation

$$\omega_0^2 = gk, \tag{1}$$

where $k = \sqrt{l(l+1)}/R_s$ is the horizontal wavevector, $R_s = 696$ Mm is the solar radius, and l is the spherical degree. This dispersion relation shows that the classical *f*-mode frequency is independent of the internal structure of the Sun.

The high accuracy (~ 0.2%) observations of the *f*-mode by Libbrecht et al. (1990), Rhodes et al. (1991), Fernandes et al. (1992), Bachmann et al. (1995), and Duvall et al. (1998) have shown that its frequency for high value of l is substantially lower than follows from parabolic dispersion relation (1).

Murawski & Roberts (1993b), Rosenthal & Gough (1994), and Rosenthal & Christensen-Dalsgaard (1995) have suggested that the *f*-mode is a surface gravity wave and attempted to explain observed *f*-mode frequency shifts. The frequencies of the interfacial *f*-mode differ from those of the classical *f*-mode only at very high spherical degree. These shifts can be used to verify the structure of the atmosphere. As a consequence of that the *f*-mode can serve as a diagnostic tool of the solar atmosphere.

The *f*-mode is also influenced by other effects. For example, Pinter & Goossens (1999) have shown that the *f*-mode frequencies are increased by a horizontal magnetic field in the solar chromosphere. On the other hand, Vanlommel & Cadez (1998) and Vanlommel & Goossens (1999) discussed the effect of frequency shift due to variations in the temperature profile. Ghosh et al. (1995) have proved that flows produce decreases of the *f*-mode frequency. Murawski & Roberts (1993a,b), Murawski & Goossens (1993), Gruzinov (1998), and Murawski et al. (1998) discussed the models in which the *f*-mode is scattered by granulation, modeled as a turbulent velocity field that is located in the convection zone. This process makes transfer of coherent energy into incoherent energy by exciting random waves and results in attenuation of the *f*-mode and consequently in line broadening. The random scattering will also affect the phase of the mode; hence the phase speed is changed (Pelinovsky et al. 1998).

Murawski et al. (1998) and Mędrek et al. (1999) generalized the above mentioned models for the case of the complex frequency. Mędrek & Murawski (2000) considered the effect of various energy spectra on the frequency and line-width of the *f*-mode. In these models, the calculations were carried out for a plane-parallel equilibrium consisting of two layers in which mass densities were assumed constants, while the realistic model of the solar atmosphere should take the stratification into account.

The main goal of this paper is to examine the influence of stratification and turbulence on frequencies and line-widths of the solar *f*-mode. To do so, we present a generalization of the model developed by Murawski & Roberts (1993a,b) to the case of a stratified atmosphere and convection zone, and explain the frequency reduction and wave damping of the *f*-mode.

We start by setting up the problem in Sect. 2, where we describe the physics included in our equations. In Sect. 3, we derive the dispersion relation for the non-turbulent *f*-mode and consider as an illustrative example the case of isothermal plasma. Sect. 4

Send offprint requests to: kamur@akropolis.pol.lublin.pl

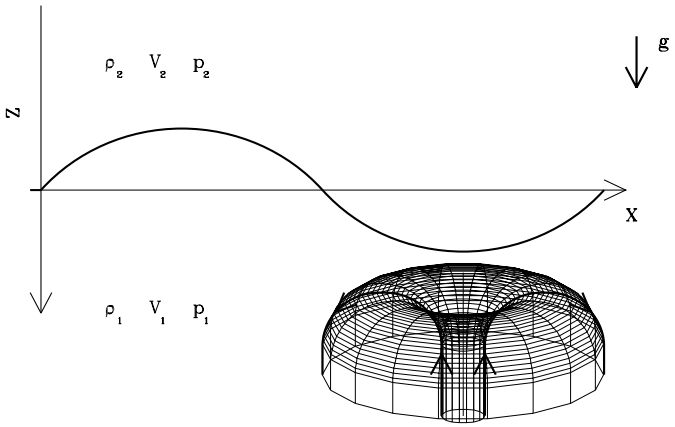

Fig. 1. The geometry of the problem. The chromosphere and solar corona occupy the upper half-plane. The photosphere and convection zone occur at > 0. The convective random flow is located at the lower half-plane and the *f*-mode is represented by the sinusoidal line.

presents the dispersion relation for the turbulent *f*-mode. In the following section, we investigate the influence of turbulence and equilibrium structure on the frequencies and line-widths of the solar *f*-mode. We compare these frequencies and line-widths with the results of recent observations by the SOHO/MDI.

2. Setup of the problem

In this section, we consider the *f*-mode that propagates along an interface between two semi-infinite layers of perfect gas of equilibrium density $\varrho_0(z)$ and temperature $T_0(z)$, stratified under gravity, g, which is taken to be pointing in the z-direction (Fig. 1). The coordinate z decreases with height.

The lower layer ($z > 0$) represents the convection zone and the overlaying photosphere. The upper layer represents the chromosphere and solar corona which occupy the half-space $z < 0$. The flow quantities below the interface (for $z > 0$) are denoted by the subscript 1, while these quantities above the interface (for $z < 0$) are distinguished by the subscript 2. The interface is taken to be located at $z = 0$. This model is a special case of the model which was considered by Vanlommel & Cadez (1998) and Vanlommel & Goossens (1999) (valid for the width of the chromosphere, $L = 0$).

Furthermore, we apply the Cowling approximation (Cowling 1941) according to which perturbations to the gravity field are ignored. As long as $l > 50$ this is a valid assumption. The solar curvature is negligible as long as $l \gg 0$. Under these assumptions the Sun can be modeled as plane-parallel with constant gravity g.

It is assumed that the *f*-mode is incompressible and the plasma is magnetic field-free, *i. e.* the motions in the solar atmosphere are described by hydrodynamic equations, viz.

$$\varrho_{,t} + \nabla \cdot (\varrho \boldsymbol{V}) = 0, \tag{2}$$

$$\nabla \cdot \boldsymbol{V} = 0, \tag{3}$$

$$\varrho[\boldsymbol{V}_{,t} + (\boldsymbol{V} \cdot \nabla)\boldsymbol{V}] = -\nabla p + \varrho \boldsymbol{g}, \tag{4}$$

together with the boundary conditions at the interface,

$$p_1 = p_2, \qquad \text{at } z = \eta(x,t), \tag{5}$$

$$(\partial_t + \boldsymbol{V} \cdot \nabla)(\eta - z) = 0, \qquad \text{at } z = \eta. \tag{6}$$

Here, ϱ is the mass density, $\boldsymbol{V}$ is the velocity, p is the pressure, g is the gravitational acceleration and $z = \eta(x,t)$ describes the wavy interface. Henceforth, indices with the comma denote the partial derivatives, e.g. $\boldsymbol{V}_{,t} \equiv \frac{\partial \boldsymbol{V}}{\partial t}$.

In what follows we assume two-dimensional motions with $\partial_y = 0$ and $V_y = 0$ and consider the case when the transitional layer $z = 0$ becomes a sharp discontinuity of density and temperature. In particular, we take into account the equilibrium state in which the flow $\boldsymbol{V}_0$ occurs in the lower medium only and it depends both on x, $z > 0$ and t. The mass density ϱ_0 and the pressure p_0 are functions of z only, viz.

$$\varrho_0 = \varrho_0(z), \qquad \boldsymbol{V}_0 = \boldsymbol{V}_0(x,z,t), \qquad p_0 = p_0(z). \tag{7}$$

Assuming that perturbations are small, we expand the fluid variables around this equilibrium and introduce the flux function $\psi(x,z,t)$ such that

$$V_x = -\psi_{,z}, \qquad V_z = \psi_{,x}. \tag{8}$$

3. Dispersion relation for the static ($\boldsymbol{V}_0 = 0$) atmosphere

To obtain the dispersion relation for the static ($\boldsymbol{V}_0 = 0$) atmosphere we Fourier analyze the perturbation variables as:

$$\phi(x,z,t) = \phi_0(z) e^{i(kx - \omega t)}, \quad \eta(x,t) = \eta_0 e^{i(kx-\omega t)}, \tag{9}$$

where $\eta_0 = const$, k is the horizontal wavenumber and ω is the frequency of the *f*-mode. ϕ represents a fluid variable such as ϱ, ψ and p.

From linearized Eqs. (2) - (4) we obtain the equation which describes vertical profiles of the flux function ψ, viz.

$$\psi_{,zz} + \frac{\varrho_{0,z}}{\varrho_0}\psi_{,z} + \left(g\frac{k^2}{\omega^2}\frac{\varrho_{0,z}}{\varrho_0} - k^2 \right)\psi = 0. \tag{10}$$

Boundary conditions (5) and (6) lead then to the dispersion relation

$$\omega^2(\varrho_{01}\psi_{1,z} - \varrho_{02}\psi_{2,z}) = gk^2(\varrho_{02} - \varrho_{01})\psi_1, \quad z = 0, \tag{11}$$

$$\psi_1 = \psi_2, \qquad z = 0. \tag{12}$$

From this dispersion relation it follows that the *f*-mode frequency depends on the density and mode profiles either side of the interface, the wavevector k and the gravity g.

3.1. An instructive example: The case of isothermal plasma

Similarly to Gruzinov (1998), we consider the case of uniform temperatures inside the solar corona and the solar interior. However, there is a temperature jump at the interface $z = 0$. Then, the density profiles can be written as

$$\varrho_{01} = \bar{\varrho}_1 e^{\frac{z}{h_1}}, \qquad \varrho_{02} = \bar{\varrho}_2 e^{\frac{z}{h_2}}, \tag{13}$$

where h_1 and h_2 are the isothermal pressure scale heights, $h_j = \frac{c_j^2}{\gamma g}, \quad j = 1, 2$. Here, c_1 and c_2 are the sound speeds. Consequently, there is a jump in the mass density ($\varrho_{01} \neq \varrho_{02}$) and the sound speed ($c_1 \neq c_2$) at the interface $z = 0$.

Eq. (10) then leads to

$$\psi_1 = \psi_0 e^{-b_1 z}, \quad \psi_2 = \psi_0 e^{b_2 z}, \tag{14}$$

where:

$$b_1 = \frac{\omega + \sqrt{\omega^2 + 4h_1 k^2(\omega^2 h_1 - g)}}{2h_1\omega}, \tag{15}$$

$$b_2 = \frac{-\omega + \sqrt{\omega^2 + 4h_2 k^2(\omega^2 h_2 - g)}}{2h_2\omega}. \tag{16}$$

From these equations it follows that there are cut-offs in ω below which b_1 and b_2 are complex and the wave is propagating along the z-direction. We have the following conditions for b_1 and b_2 to be real:

$$\omega^2 \geq \frac{4h_j g k^2}{1 + 4h_j^2 k^2}, \quad j = 1, 2. \tag{17}$$

In the case when this condition is not satisfied, waves cease to be localized, they propagate and the corona and the convection zone act as sinks for such perturbations.

Substituting the spatial profiles which are described by Eqs. (13) and (14) into Eq. (11) the dispersion relation for the isothermal atmosphere can be written as follows:

$$\omega^2(b_2\kappa + b_1) = g(1 - \kappa)k^2, \tag{18}$$

where the density contrast is given by

$$\kappa = \frac{\bar{\varrho}_2}{\bar{\varrho}_1}.$$

It is worth mentioning that for the case of the constant density atmosphere we have $h_1, h_2 \to \infty$ and $b_1 = b_2 = k$. Consequently, the dispersion relation takes the form:

$$\omega^2 \to gk\frac{1 - \kappa}{1 + \kappa}|_{h_1, h_2 \to \infty}. \tag{19}$$

4. Dispersion relation for the turbulent ($V_0 \neq 0$) plasma

The solar plasma below the visible layers is a dynamic environment, supporting convection which reveals itself principally on two spatial scales of motion: a large scale supergranulation with horizontal scale of $3 \cdot 10^4$ km and flows of $0.1 - 0.4$ km/s and much smaller scale granulation with horizontal scale of $0.2 - 2 \cdot 10^3$ km and flows of $1 - 3$ km/s (Simon et al. 1991). Temporal scales associated with these motions range from 30 minutes for granule overturn times to weeks for giant cells. Such dynamic medium is expected to influence the *f*-mode.

We consider a model in which weak turbulent field is settled in the convection zone. This assumption is valid since the turbulence reveals speeds ~ 1 km/s which are small in comparison to the sound speed ~ 7 km/s. Consequently, we can use the following expansion:

$$\begin{aligned} \phi(x, z, t) &= \langle \phi(x, z, t) \rangle + \phi'(x, z, t), \\ \langle \phi'(x, z, t) \rangle &= 0, \end{aligned} \tag{20}$$

where $\langle \phi(x, z, t) \rangle$ and $\phi'(x, z, t)$ represent coherent and random fields, respectively. The symbol $\langle\rangle$ denotes ensemble averaging (e.g., Ishimaru 1978). Substituting this expansion into linearized Eqs. (2)-(6) after lengthy algebra in which the binary collision approximation (Howe 1971) has been used, we obtain the dispersion relation

$$\begin{aligned} &\frac{\omega}{k}\left[\varrho_{01}\langle\psi_{1,z}(k,\omega,z)\rangle - \varrho_{02}\langle\psi_{2,z}(k,\omega,z)\rangle\frac{\langle\psi_1(k,\omega,z)\rangle}{\langle\psi_2(k,\omega,z)\rangle}\right] \\ &\quad + (\varrho_{01} - \varrho_{02})g\frac{k}{\omega}\langle\psi_1(k,\omega,z)\rangle \\ &= \int_{-\infty}^{+\infty}\Bigg\{ i\varrho_{02}\langle\psi_{2,z}(k,\omega,z)\rangle\frac{\omega}{\bar{\omega}}\frac{\bar{k}}{k^2}\frac{\psi_2'(\bar{k},\bar{\omega},z)}{\langle\psi_2(k,\omega,z)\rangle} \\ &\qquad \times\left(i\bar{k}\bar{F}\langle V_{0x}d_2\rangle - \bar{F}\langle V_{0z,z}d_2\rangle\right) \\ &\qquad + \bar{F}\langle D_1 d_1\rangle\psi_1'(\bar{k},\bar{\omega},z)_{,z} \\ &\qquad - \frac{\bar{k}}{k}\varrho_{01}\bar{F}\langle V_{0x,z}d_1\rangle\psi_1'(\bar{k},\bar{\omega},z) \\ &\qquad - \frac{\bar{k}}{\bar{\omega}}\bar{F}\langle D_2 d_2\rangle\psi_2'(\bar{k},\bar{\omega},z)\Bigg\}d\bar{k}d\bar{\omega}, \quad z = 0. \end{aligned} \tag{21}$$

The functions $\langle\psi_j\rangle$ and ψ_j, $j = 1, 2$, are solutions of Eq. (10). The formulae which determine the right hand side of this equation are presented in Appendix A. Here, $\bar{F}$ denotes the Fourier transform operator evaluated at $k - \bar{k}$ and $\omega - \bar{\omega}$.

From dispersion relation (21) it follows that the dependence of the cyclic frequency ω on the wavevector k differs from non-turbulent dispersion relation (11). The turbulent field changes the *f*-mode frequency. This change is described by the real part of ω. As a consequence of scattering by turbulent flow, the energy of the *f*-mode is partially transformed into the turbulent field (Pelinovsky et al. 1998). This phenomenon is associated with the imaginary part of the frequency, $\mathrm{Im}(\omega)$.

5. Numerical results

In this section we consider the numerical solutions of dispersion relation (21) for an illustrative example of the isothermal atmosphere (Gruzinov 1998). Henceforth, we assume that the turbulent flow is time-independent. This assumption is valid for the wave period T which is much lower than the turnover time T_c, viz. $T \ll T_c = 30\,\mathrm{min}$. Hence, we get a corresponding condition for the frequency $\nu \equiv 1/T \gg 600\,\mu\mathrm{Hz}$. Consequently, our model is valid for sufficiently high frequencies.

As an illustrative case we take

$$V_{0x}(x, z) = e^{-\alpha z}u_0(x), \quad V_{0z}(x, z) = -ze^{-\alpha z}u_{0,x}(x), \tag{22}$$

where $\alpha > 0$ is the flow penetration factor. Consequently, the vertical flow disappears at $z = 0$.

The correlation function is assumed to be Gaussian

$$\langle u_0(x)u_0(X)\rangle = \sigma^2 e^{-\frac{(X-x)^2}{4l_x^2}}, \tag{23}$$

where l_x is the correlation length and σ is the variance. For a description of the solar turbulence the reader is referred to

Canuto & Christensen-Dalsgaard (1998). The Fourier transform of this correlation function is equal to

$$F\left\langle u_0(x)u_0(X)\right\rangle = \frac{\sigma^2 l_x}{\pi} e^{-k^2 l_x^2}. \quad (24)$$

We use the following values for the surface gravity $g = 274$ m/s^2 and the polytropic index $\gamma = 5/3$. In the following figures, the frequency $\nu = Re(\omega)/2\pi$ and the line-width $\Gamma = -2Im(\omega)$ (e.g., Osaki 1990) are displayed as functions of the spherical harmonic l for various parameters of the equilibrium and turbulent flow. The SOHO/MDI data (Duvall et al. 1998) is shown by the dotted curve for comparison purposes.

First, we illustrate a dependence of the numerically obtained results on the equilibrium parameters such as the density contrast κ, the photospheric pressure scale height h_1, and the temperature ratio

$$\delta = \frac{T_2(z=0)}{T_1(z=0)}$$

which determines the coronal pressure scale height, $h_2 = h_1\delta$. Then, we show our results as functions of the flow parameters: the variance σ, the correlation length l_x, and the penetration factor α.

Fig. 2 presents the computed frequency ν and the line-width Γ as functions of the angular degree l for two values of the density contrast: $\kappa = 0.1$ (solid line) and $\kappa = 0.001$ (broken line). The dotted line represents the SOHO/MDI data (Duvall et al. 1998). The broken line of the frequency ν lies above the solid line and it fits better the SOHO/MDI data. The *f*-mode exists only if its modal frequencies are higher than the cut-off frequencies which are described by Eq. (17). In this case it is a mode which is localized in the vertical direction z. At frequencies below these cut-offs, the solar corona and the convection zone become transparent and the mode is not localized anymore. Instead, the *f*-mode can propagate through these regions and it leaks away. It is not an eigen-mode that persists in time. As a consequence of that the computed frequencies do not exist for low values of l. The line-width corresponding to $\kappa = 0.001$ (broken line) is higher than the line-width for $\kappa = 0.1$ (solid line) for overall values of l. These lines lie close to the observational data (dotted line). These theoretical curves cross the observational line at $l \simeq 1300$.

Fig. 3 shows the frequency ν and the line-width Γ for $h_1 = 500$ km (solid line) and $h_1 = 50000$ (broken line). The latter case corresponds to a weakly stratified atmosphere and convection zone. In particular, the case of $h_1 \to \infty$ is associated with a homogeneous atmosphere and convection zone. This case was discussed by Mędrek et al. (1999). The broken frequency line lies below the solid line which fits better the SOHO/MDI data. It is interesting to note that for the case of $h_1 = 50000$ km the *f*-mode exists for the entire range of l while at $l \simeq 1100$ the solid curve exhibits a cut-off which corresponds to unstable ($Im(\omega) > 0$) *f*-mode. The line-width corresponding to $h_1 = 50000$ km (broken line) is higher than the line-width for $h_1 = 500$ km (solid line). Although the solid line lies below the observational curve it is close to the SOHO/MDI data (dotted line). The broken curve exhibits a maximum at $l \simeq 1600$. The results for large h_1 are in agreement with the work by Mędrek et al. (1999).

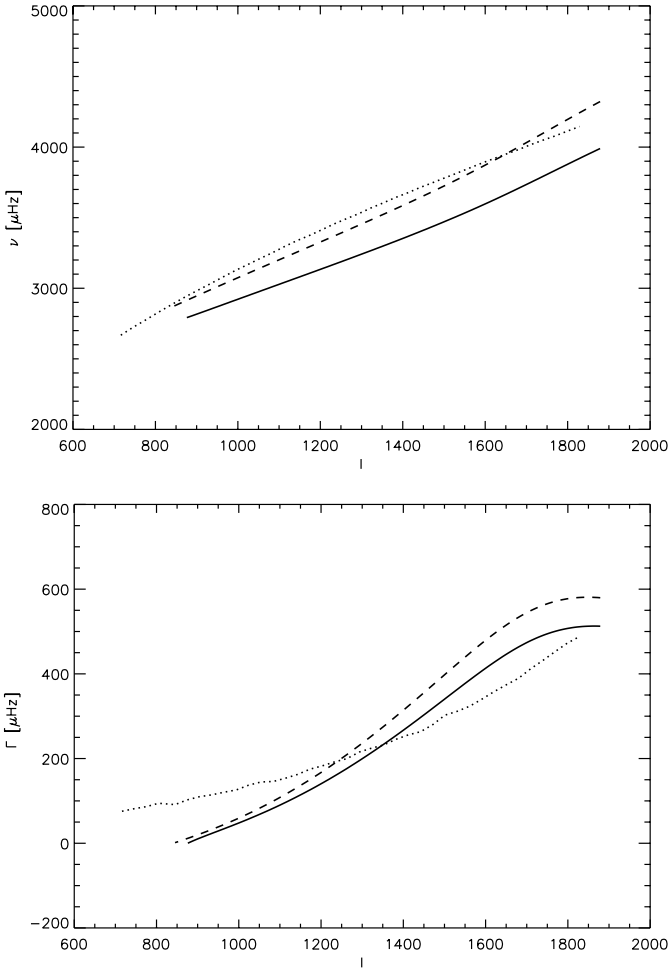

Fig. 2. The frequency ν and the line-width Γ of the solar *f*-mode as a function of the angular degree l for the density ratio $\kappa = 0.01$ (solid curve) and $\kappa = 0.001$ (broken curve). The other equilibrium parameters are $\delta = 167$ and $h_1 = 10^3$ km. A turbulent flow is characterized by the correlation length $l_x = 600$ km, the variance $\sigma = 3$ km/s and the penetration factor $\alpha = 1/l_x$. The SOHO/MDI data is represented by the dotted curve.

Fig. 4 presents ν and Γ for the variance $\sigma = 1$ km/s (solid line) and $\sigma = 5$ km/s (broken line). The effect of a stronger turbulent flow is to reduce more the frequency of the *f*-mode and to increase the line-width (Murawski et al. 1998). As a consequence of that the broken curve lies below the solid line which is close to the observational data. The line-width corresponding to $\sigma = 5$ km/s (broken line) is higher that the line-width for $\sigma = 1$ km/s (solid line). For the influence of σ on the line-width see also Murawski et al. (1998), Mędrek & Murawski (2000), and Mędrek et al. (1999).

Fig. 5 shows the frequency ν and the line-width Γ for the correlation length $l_x = 200$ km (solid line) and $l_x = 2000$ km (broken line). A better fit to the SOHO/MDI data is obtained for the case of $l_x = 2000$ km. The line-width exhibits the min-

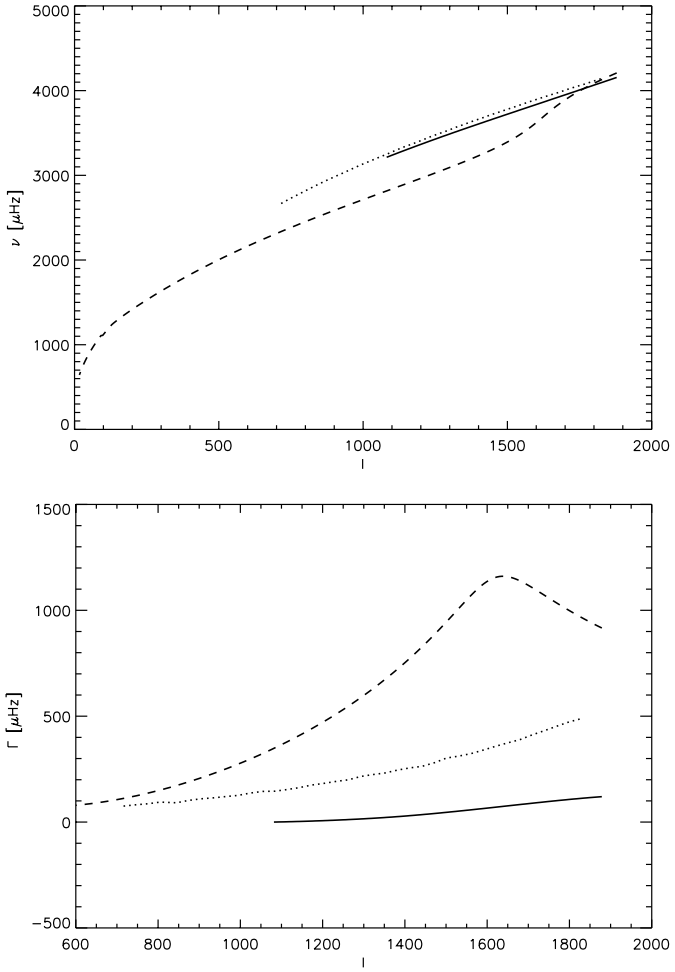

Fig. 3. Dispersion curves for $h_1 = 500$ km (solid curve) and $h_1 = 50000$ km (broken curve). The other parameters are: $\delta = 167$, $\kappa = 0.05$, $l_x = 600$ km, $\sigma = 3$ km/s and $\alpha = 1/l_x$. The SOHO/MDI data is represented by the dotted curve.

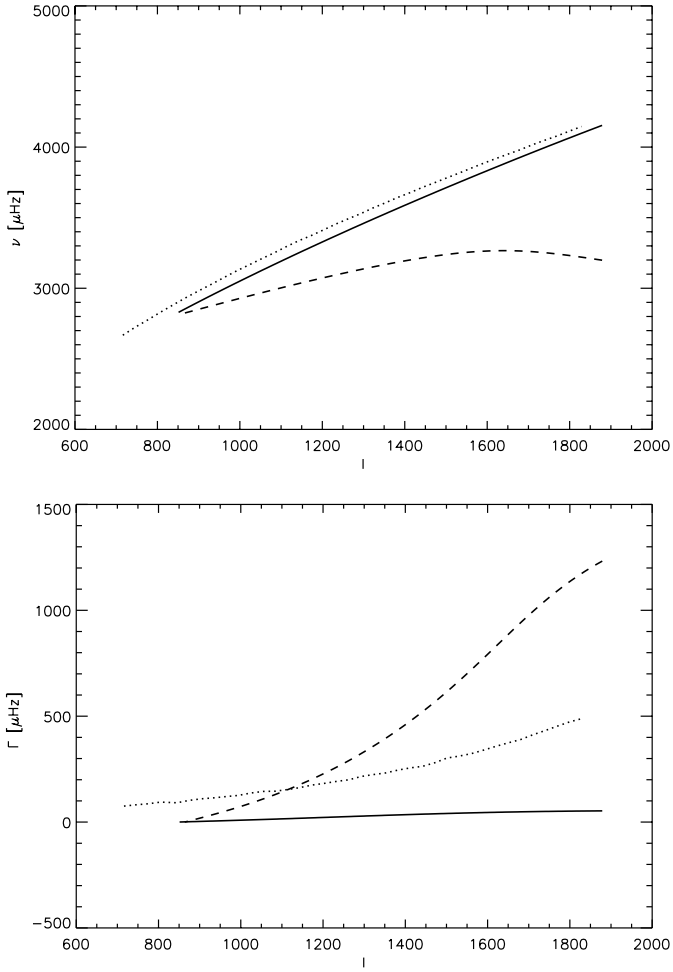

Fig. 4. Dispersion curves for $\sigma = 1$ km/s (solid curve) and $\sigma = 5$ km/s (broken curve) and $\delta = 167$, $\kappa = 0.05$, $h_1 = 1000$ km, $l_x = 600$ km, and $\alpha = 1/l_x$. The SOHO/MDI data is represented by the dotted curve.

imum and maximum at $l \simeq 700$ and $l \simeq 100$, respectively. Consequently, smaller granules decrease more the frequency and broaden the line-width. An averaging of the results over different l_x leads to a better agreement between the theoretical and observational results (Mędrek & Murawski 2000).

Fig. 6 illustrates ν and Γ for the flow penetration factor $\alpha = 2/l_x$ (solid line) and $\alpha = 1/2l_x$ (broken line). A larger value of α corresponds to the flow which is more confined to the unperturbed interface $z = 0$. While both the solid and broken lines are close to the observational data, a better fit to the SOHO/MDI line-width is obtained for $\alpha = 2/l_x$. A larger value of α reduces more the frequency but essentially it increases the line-width. These results are in an agreement with the work by Murawski & Roberts (1993b).

Fig. 7 shows imaginary parts of $b_1 l_x$ (solid line) and $b_2 l_x$ (dotted line) for the turbulent *f*-mode. As the imaginary parts differ from zero the *f*-mode leaks into the solar corona and the solar interior. This leakage is higher into the solar interior as $|Im(b_1)| > |Im(b_2)|$. Consequently, the wave profiles are no longer purely exponential but are oscillatory in the z-direction. The envelopes of these oscillations in the convection zone and the solar corona are exponentials: $e^{-Re(b_1)z}$ and $e^{Re(b_2)z}$, respectively.

6. Conclusions

Our purpose was not to make extremely accurate matching of the theoretical and observational data. Instead, we designed a simple model of the solar atmosphere to show up trends and general properties caused by the turbulent velocity field. In accordance with this purpose we made several assumptions and simplifications. For example, we ignored sphericity, variation of g and γ, magnetic fields and nonadiabatic effects.

We constructed a solar model consisting of two regions. The lower region corresponds to the solar interior and photosphere. The upper region is the solar corona and chromosphere. The *f*-mode is a surface gravity wave which for $l < 1500$ is peaked in amplitude below the solar surface (Rosenthal & Christensen-Dalsgaard 1995, Pinter & Goossens 1999).

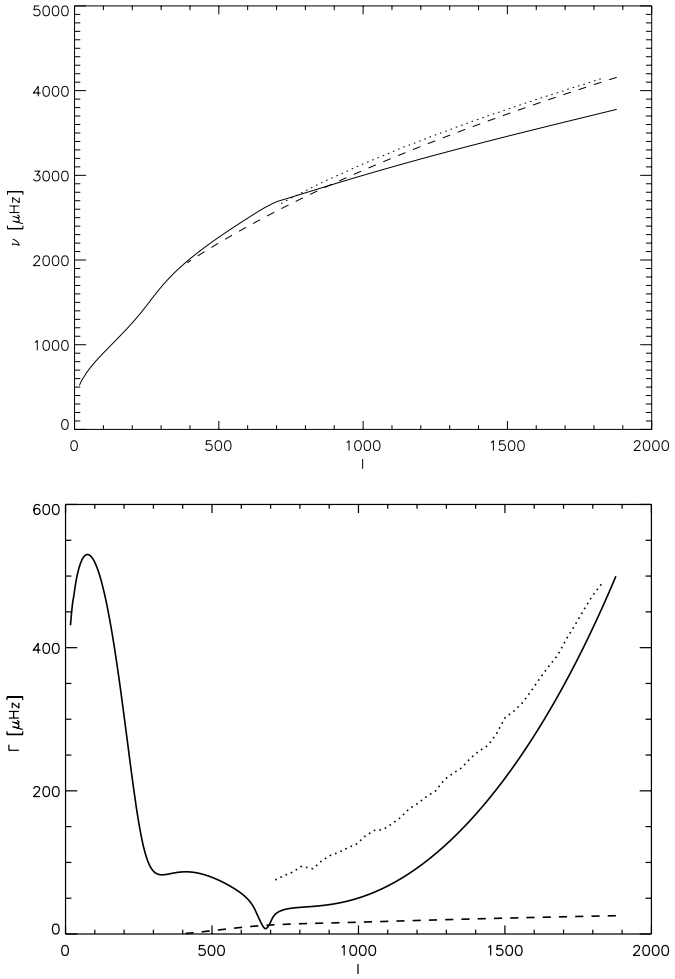

Fig. 5. Dispersion curves for $l_x = 200$ km (solid curve) and $l_x = 2000$ km (broken curve) and $\delta = 167$, $\kappa = 0.05$, $h_1 = 1000$ km, $\sigma = 3$ km/s and $\alpha = 1/l_x$. The SOHO/MDI data is represented by the dotted curve.

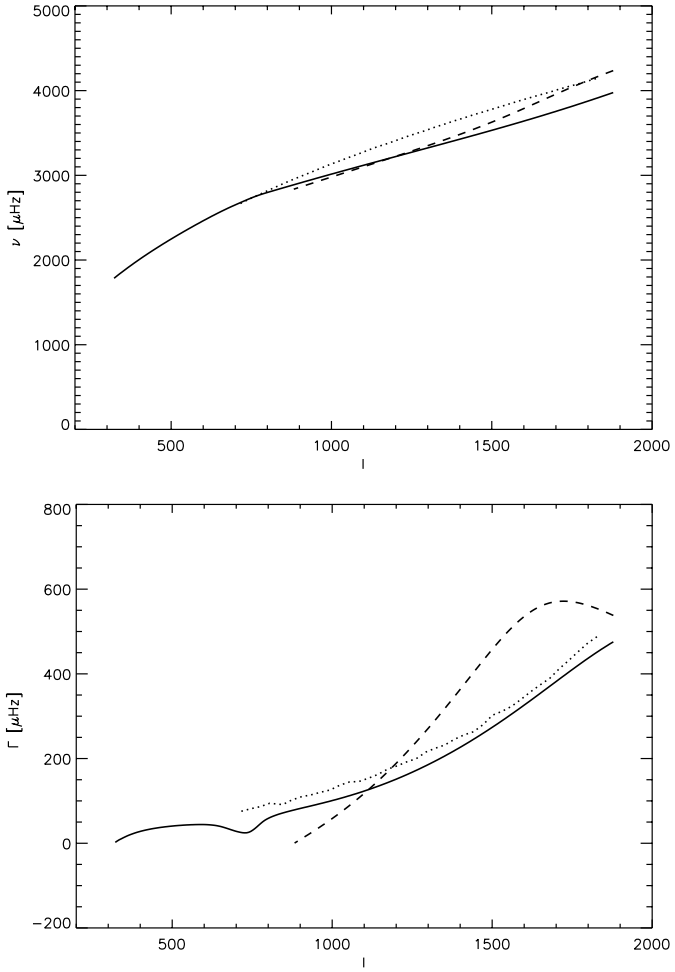

Fig. 6. Dispersion curves for $\alpha = 2/l_x$ (solid curve) and $\alpha = 0.5/l_x$ (broken curve). The other parameters are: $\delta = 167$, $\kappa = 0.05$, $h_1 = 1000$ km, $\sigma = 3$ km/s, and $l_x = 600$ km. The SOHO/MDI data is represented by the dotted curve.

Moreover, our model of the solar atmosphere is highly idealized. It is intended merely to be illustrative of the physics of the interfacial mode in a continuously stratified atmosphere. A plausible model would have to include the details of the structure of the chromosphere (e.g. Pinter & Goossens 1999). Therefore, it is clearly desirable to extend these models to more realistic stratifications of the solar atmosphere.

Although the obtained results are for a specific equilibrium (isothermal plasma) and turbulent flow, dispersion relation (21) is valid for arbitrary equilibrium profiles and turbulent flow. Moreover, the methodology we introduced to derive this equation can be applied to any model of the solar atmosphere. Although details of the effects of different models will vary, the general character of the effects that we stressed here are expected to be the same.

Despite of its shortcomings such as the assumption of isothermal convection zone, our simple model of the solar atmosphere and turbulent velocity field is able to give similar results to those observed by the SOHO/MDI instrument (Duvall et al. 1998) as well as agree with alternative explanations of the frequency shift due to magnetized atmosphere (Pinter & Goossens 1999) and variations in the temperature profile (Vanlommel & Cadez 1998, Vanlommel & Goossens 1999). Qualitatively all these effects influence the *f*-mode frequency in the same way. The overall agreement of the model frequency with the experimental data and former results offers encouragement for the further studies of the influence of the convection on the *f*-mode frequencies.

Acknowledgements. The author expresses his cordial thanks to Dr. Valera Nakariakov, Dr. Michael Ruderman, Prof. Bernard Roberts and Prof. Efim Pelinovsky for stimulating discussions. This work was financially supported by the State Committee for Scientific Research in Poland, KBN grant no. 2 PO3D 017 17. The numerical simulations have been performed on an Sun workstation at the Institute of Physics, UMCS Lublin and on a SGI power station at the Poznan Supercomputing Center.

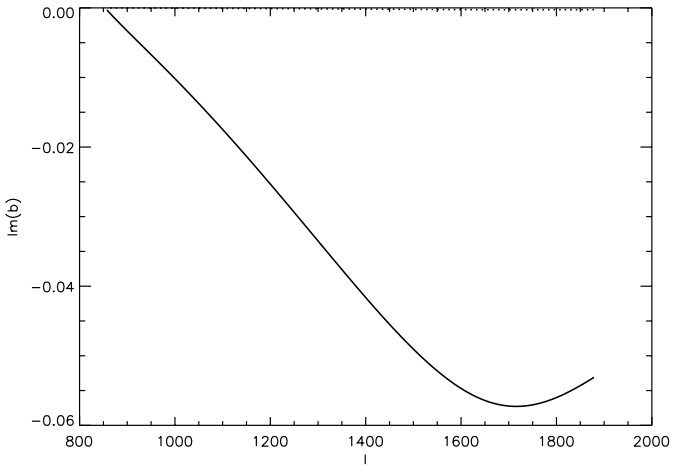

Fig. 7. The imaginary part of $b_1 l_x$ (solid curve) and $b_2 l_x$ (dotted curve) for the *f*-mode as functions of the angular degree l for $\kappa = 0.05$, $\delta = 167$, $h_1 = 10^3$ km, $l_x = 600$ km, $\sigma = 3$ km/s, and $\alpha = 1/l_x$.

Appendix A: Formulae for dispersion relation (21)

The right hand side of turbulent dispersion relation (21) contains the following relations:

$$W = \varrho_{01}\psi_2'(\bar{k},\bar{\omega},z)\psi_1'(\bar{k},\bar{\omega},z)_{,z} - \varrho_{02}\psi_1'(\bar{k},\bar{\omega},z)\psi_2'(\bar{k},\bar{\omega},z)_{,z} + \frac{\bar{k}^2}{\bar{\omega}^2}(\varrho_{01}-\varrho_{02})g\psi_2'(\bar{k},\bar{\omega},z)\psi_1'(\bar{k},\bar{\omega},z), \quad \text{(A.1)}$$

$$\bar{F}\langle V_{0x}d_2\rangle W = \frac{\bar{k}}{\bar{\omega}}\psi_1'(\bar{k},\bar{\omega},z)\left[\bar{F}\langle V_{0x}B_1\rangle\langle\psi_1(k,\omega,z)_{,z}\rangle + \bar{F}\langle V_{0x}B_3\rangle\langle\psi_1(k,\omega,z)\rangle\right] + i\frac{\bar{k}}{\bar{\omega}^2}\left[\frac{\bar{\omega}}{\bar{k}}\varrho_{01}\psi_1'(\bar{k},\bar{\omega},z)_{,z} + \frac{\bar{k}}{\bar{\omega}}(\varrho_{01}-\varrho_{02})g\psi_1'(\bar{k},\bar{\omega},z)\right] \times\left(\bar{F}\langle V_{0x}V_{0z,z}\rangle - ik\bar{F}\langle V_{0x}V_{0x}\rangle\right)\left\langle\psi_1(\bar{k},\bar{\omega},z)\right\rangle, \quad \text{(A.2)}$$

$$\bar{F}\langle V_{0z,z}d_2\rangle W = \frac{\bar{k}}{\bar{\omega}}\psi_1'(\bar{k},\bar{\omega},z)\left[\bar{F}\langle V_{0z,z}B_1\rangle\langle\psi_1(k,\omega,z)_{,z}\rangle + \bar{F}\langle V_{0z,z}B_3\rangle\langle\psi_1(k,\omega,z)\rangle\right] + i\frac{\bar{k}}{\bar{\omega}^2}\left[\frac{\bar{\omega}}{\bar{k}}\varrho_{01}\psi_1'(\bar{k},\bar{\omega},z)_{,z} + \frac{\bar{k}}{\bar{\omega}}(\varrho_{01}-\varrho_{02})g\psi_1'(\bar{k},\bar{\omega},z)\right] \times\left(\bar{F}\langle V_{0z,z}V_{0z,z}\rangle - ik\bar{F}\langle V_{0z,z}V_{0x}\rangle\right)\left\langle\psi_1(\bar{k},\bar{\omega},z)\right\rangle, \quad \text{(A.3)}$$

$$\bar{F}\langle V_{0x}B_1\rangle = \frac{k}{\bar{k}}\varrho_{01}\bar{F}\langle V_{0x}V_{0x}\rangle - \frac{i}{\bar{k}}\varrho_{01}\bar{F}\langle V_{0x}V_{0x,x}\rangle, \quad \text{(A.4)}$$

$$\bar{F}\langle V_{0z,z}B_1\rangle = \frac{k}{\bar{k}}\varrho_{01}\bar{F}\langle V_{0z,z}V_{0x}\rangle - \frac{i}{\bar{k}}\varrho_{01}\bar{F}\langle V_{0z,z}V_{0x,x}\rangle, \quad \text{(A.5)}$$

$$\bar{F}\langle V_{0x}B_3\rangle = -\frac{k}{\bar{k}}\varrho_{01}\bar{F}\langle V_{0x}V_{0x,z}\rangle - i\frac{k}{\bar{\omega}\omega}(\varrho_{01}-\varrho_{02})g\left(\bar{F}\langle V_{0x}V_{0z,z}\rangle - ik\bar{F}\langle V_{0x}V_{0x}\rangle\right), \quad \text{(A.6)}$$

$$\bar{F}\langle V_{0z,z}B_3\rangle = -\frac{k}{\bar{k}}\varrho_{01}\bar{F}\langle V_{0z,z}V_{0x,z}\rangle - i\frac{k}{\bar{\omega}\omega}(\varrho_{01}-\varrho_{02})g(\bar{F}\langle V_{0z,z}V_{0z,z}\rangle - ik\bar{F}\langle V_{0z,z}V_{0x}\rangle), \quad \text{(A.7)}$$

$$\bar{F}\langle D_1 d_1\rangle W = \frac{\varrho_{01}}{k}(\bar{k}\bar{F}\langle V_{0x}W_{10}\rangle - i\bar{F}\langle V_{0x,x}W_{10}\rangle), \quad \text{(A.8)}$$

$$\bar{F}\langle V_{0x}W_{10}\rangle = \frac{i}{\bar{\omega}}\varrho_{02}\psi_{02}'(\bar{k},\bar{\omega},z)_{,z}\left\langle\psi_1(\bar{k},\bar{\omega},z)\right\rangle \times\left(\bar{F}\langle V_{0x}V_{0z,z}\rangle - ik\bar{F}\langle V_{0x}V_{0x}\rangle\right) + \frac{\bar{k}}{\bar{\omega}}\psi_{02}'(\bar{k},\bar{\omega},z)\left(\bar{F}\langle V_{0x}B_1\rangle\langle\psi_1(k,\omega,z)_{,z}\rangle + \bar{F}\langle V_{0x}B_3\rangle\langle\psi_1(k,\omega,z)\rangle\right), \quad \text{(A.9)}$$

$$\bar{F}\langle V_{0x,x}W_{10}\rangle = \frac{i}{\bar{\omega}}\varrho_{02}\psi_{02}'(\bar{k},\bar{\omega},z)_{,z}\left\langle\psi_1(\bar{k},\bar{\omega},z)\right\rangle \times\left(\bar{F}\langle V_{0x,x}V_{0z,z}\rangle - ik\bar{F}\langle V_{0x,x}V_{0x}\rangle\right) + \frac{\bar{k}}{\bar{\omega}}\psi_{02}'(\bar{k},\bar{\omega},z)\left(\bar{F}\langle V_{0x,x}B_1\rangle\langle\psi_1(k,\omega,z)_{,z}\rangle + \bar{F}\langle V_{0x,x}B_3\rangle\langle\psi_1(k,\omega,z)\rangle\right), \quad \text{(A.10)}$$

$$\bar{F}\langle V_{0x,x}B_1\rangle = \frac{\varrho_{01}}{\bar{k}}(k\bar{F}\langle V_{0x,x}V_{0x}\rangle - i\bar{F}\langle V_{0x,x}V_{0x,x}\rangle), \quad \text{(A.11)}$$

$$\bar{F}\langle V_{0x,x}B_3\rangle = -\frac{k}{\bar{k}}\varrho_{01}\bar{F}\langle V_{0x,x}V_{0x,z}\rangle - i\frac{k}{\bar{\omega}\omega}(\varrho_{01}-\varrho_{02})g \times\left(\bar{F}\langle V_{0x,x}V_{0z,z}\rangle - ik\bar{F}\langle V_{0x,x}V_{0x}\rangle\right), \quad \text{(A.12)}$$

$$\bar{F}\langle V_{0x,z}d_1\rangle W = \frac{i}{\bar{\omega}}\varrho_{02}\psi_{02}'(\bar{k},\bar{\omega},z)_{,z}(\bar{F}\langle V_{0x,z}V_{0z,z}\rangle - ik\bar{F}\langle V_{0x,z}V_{0x}\rangle)\left\langle\psi_1(\bar{k},\bar{\omega},z)\right\rangle + \frac{\bar{k}}{\bar{\omega}}\psi_{02}'(\bar{k},\bar{\omega},z)(\bar{F}\langle V_{0x,z}B_1\rangle\langle\psi_1(k,\omega,z)_{,z}\rangle + \bar{F}\langle V_{0x,z}B_3\rangle\langle\psi_1(k,\omega,z)\rangle), \quad \text{(A.13)}$$

$$\bar{F}\langle V_{0x,z}B_1\rangle = \frac{k}{\bar{k}}\varrho_{01}\bar{F}\langle V_{0x,z}V_{0x}\rangle - \frac{i}{\bar{k}}\varrho_{01}\bar{F}\langle V_{0x,z}V_{0x,x}\rangle, \quad \text{(A.14)}$$

$$\bar{F}\langle V_{0x,z}B_3\rangle = -\frac{k}{\bar{k}}\varrho_{01}\bar{F}\langle V_{0x,z}V_{0x,z}\rangle - i\frac{k}{\bar{\omega}\omega}(\varrho_{01}-\varrho_{02}) \times g(\bar{F}\langle V_{0x,z}V_{0z,z}\rangle - ik\bar{F}\langle V_{0x,z}V_{0x}\rangle), \quad \text{(A.15)}$$

$$\bar{F}\langle D_2 d_2\rangle W = i\frac{(\varrho_{01}-\varrho_{02})g}{\omega}W(\bar{F}\langle V_{0z,z}d_2\rangle - i\bar{k}\bar{F}\langle V_{0x}d_2\rangle). \quad \text{(A.16)}$$

References

Bachmann K.T., Duvall Jr. T.J., Harvey J.W., Hill F., 1995, ApJ 443, 837
Campbell W.R, Roberts B., 1989, ApJ 338, 538
Canuto V.M., Christensen-Dalsgaard J., 1998, Annu. Rev. Fluid Mech. 30, 167
Cowling T.G., 1941, MNRAS 101, 367
Duvall Jr. T.J., Kosovitschev A., Murawski K., 1998, ApJ 505, L55
Fernandes D.N., Scherrer P.H., Tarbell T.D., Title A.M., 1992, ApJ 392, 736
Ghosh P., Antia H.M., Chitre S.M., 1995, ApJ 451, 851
Gruzinov A.V., 1998, ApJ 498, 458
Howe M.S., 1971, J. Fluid Mech. 45, 785
Ishimaru A., 1978, Wave propagation and scattering in random media. Academic Press, New York, NY
Libbrecht K.G., Woodard M.F., Kaufman J.M., 1990, ApJS 74, 1129
Mędrek M., Murawski K., Roberts B., 1999, A&A 349, 312
Męd rek M., Murawski K., 2000, ApJ, in press
Murawski K., Goossens M., 1993, A&A 279, 225
Murawski K., Roberts B., 1993a, A&A 272, 595
Murawski K., Roberts B., 1993b, A&A 272, 601
Murawski K., Kosovitschev A.G., Duvall Jr. T.J., 1998, In: Proceed. SOHO 6/GONG 98 Workshop, Boston
Osaki Y., 1990, In: Osaki Y., Shibahashi H. (eds.) Progress of Seismology of the Sun and Stars. Lect. Not. Phys. 367, Springer, Berlin, p. 75
Pelinovsky E., Razin A.V., Sasorova E.V., 1998, Waves in Random Media 8, 255
Pinter B., Goossens M., 1999, A&A 347, 321
Rhodes E.J., Cacciani A., Korzennik S.G., 1991, Adv. Space Res. 11, (4)17
Rosenthal C.S., Christensen-Dalsgaard J., 1995, MNRAS 276, 1003
Rosenthal C.S., Gough D., 1994, ApJ 423, 488
Simon G.W., Title A.M., Weiss N.O., 1991, ApJ 375, 775
Vanlommel P., Cadez V., 1998, Solar Phys. 182, 263
Vanlommel P., Goossens M., 1999, Solar Phys. 187, 357